JACS
JOURNAL OF THE AMERICAN CHEMICAL SOCIETY
Article
pubs.acs.org/JACS

Why (1 0 0) Terraces Break and Make Bonds: Oxidation of Dimethyl Ether on Platinum Single-Crystal Electrodes

Hongjiao Li,[†,‡] Federico Calle-Vallejo,[†,§] Manuel J. Kolb,[†] Youngkook Kwon,[†] Yongdan Li,[‡] and Marc T.M. Koper*[,†]

[†]Leiden Institute of Chemistry, Leiden University, P.O. Box 9502, 2300 RA Leiden, The Netherlands

[‡]Tianjin Key Laboratory of Applied Catalysis Science and Technology and State Key Laboratory for Chemical Engineering, School of Chemical Engineering and Technology, Tianjin University, Tianjin 300072, People's Republic of China

[§]Université de Lyon, Institut de Chimie, Laboratoire de Chimie, École Normale Supérieure de Lyon, 46 Allée d'Italie, 69364 Lyon Cedex 07, France

Supporting Information

ABSTRACT: A surface structural preference for (1 0 0) terraces of fcc metals is displayed by many bond-breaking or bond-making reactions in electrocatalysis. Here, this phenomenon is explored in the electrochemical oxidation of dimethyl ether (DME) on platinum. The elementary C−O bond-breaking step is identified and clarified by combining information obtained from single-crystal experiments and density functional theory (DFT) calculations. Experiments on Pt(1 0 0), Pt(5 1 0), and Pt(10 1 0) surfaces show that the surface structure sensitivity is due to the bond-breaking step, which is unfavorable on step sites. DFT calculations suggest that the precursor for the bond-breaking step is a CHOC adsorbate that preferentially adsorbs on a square ensemble of four neighboring atoms on Pt(1 0 0) terraces, named as "the active site". Step sites fail to strongly adsorb CHOC and are, therefore, ineffective in breaking C−O bonds, resulting in a decrease in activity on surfaces with increasing step density. Our combined experimental and computational results allow the formulation of a new mechanism for the electro-oxidation of DME as well as a simple general formula for the activity of different surfaces toward electrocatalytic reactions that prefer (1 0 0) terrace active sites.

INTRODUCTION

Several important electrocatalytic reactions on metal surfaces at room temperature have in common a striking structure sensitivity displayed by exhibiting their highest catalytic activity at perfect two-dimensional (1 0 0) terraces.[1] Examples include the reduction of carbon monoxide on copper,[2−4] ammonia oxidation on platinum,[5] nitrite reduction on platinum,[6,7] dimethyl ether oxidation on platinum,[8] and oxygen reduction on gold.[9] All of these reactions have in common the breaking or making of a bond between C, N, and O, i.e., C−C, N−N, N−O, C−O, and O−O. It is expected that there is a general rule for this intriguing phenomenon, but no theory or model has yet been proposed.

This work sets out to shed light on this remarkable structure sensitivity in electrocatalysis by a combined experimental and computational study of the oxidation of dimethyl ether (DME) on a number of single-crystal surfaces of platinum in acid solution. The reason for choosing DME oxidation on platinum lies in the fact that it gives rise to simple, stable, and electrochemically visible fragments. Additionally, the previous studies of Ye et al. provide an insightful starting point for further mechanistic studies of this reaction.[8,10] Therefore, the electrochemical oxidation of DME is an excellent case study for the preference for (1 0 0) terraces in electrocatalysis. Besides, DME is a safe and clean fuel with various applications in industry and promising developments in fuel cells for portable applications.[11,12] The detailed elucidation of its oxidation mechanism would have a significant impact on the DME-related academic and applied research.

Ye et al. have thoroughly studied the surface structure sensitivity of the electrochemical oxidation of DME in sulfuric acid using well-defined platinum surfaces.[8] With the combination of in situ infrared (IR) spectroscopy and electrochemical methods, Ye et al.[13] proposed that the initial dehydrogenation of DME yields $*CH_2OCH_3$ (* denoting chemisorption), followed by the scission of the C−O bond to generate methanol and CO, both leading to CO_2, the final product. Several intermediates, in particular $*CH_2OCH_3$ and *CO, have been detected with IR by other groups.[14−16] However, no agreement has been achieved on all the reaction intermediates, and there is no complete reaction mechanism. Besides, the existing reports do not explain why the reaction prefers Pt(1 0

Received: June 30, 2013
Published: August 27, 2013

   dx.doi.org/10.1021/ja406655q | J. Am. Chem. Soc. 2013, 135, 14329−14338

0) terraces and why steps have a negative influence on the activity.

To answer the aforementioned questions, herein we combine experiments on well-defined platinum single crystals with detailed Density Functional Theory (DFT) calculations. The cleavage of the C−O bond is studied by stripping experiments that give clues on the nature of the bond-breaking fragments and the structure sensitivity of their formation. The stripping method and the corresponding identification of the decomposition fragments have been scrutinized in detail by previous stripping experiments of the electro-oxdiation of ethanol and acetaldehyde.[17] The identification of *CO and *CH as fragments was subsequently confirmed by surface-enhanced Raman Spectroscopy (SERS).[18] Since the electro-chemical oxidation of ethanol has already been extensively studied in our group[17−19] and since ethanol and DME are isomers and generate similar (if not the same) decomposition fragments, comparative experiments on ethanol have also been carried out. Our DFT calculations start with $*CH_3OC$, which was suggested as the most likely precursor of the bond-breaking step by Ye et al.[13] We will map out the energetics of the possible pathways and their structure sensitivity. Significantly, our studies converge to the existence of a special active site for the bond-breaking step that optimally utilizes the square symmetry of the (1 0 0) terrace. We believe that this finding has relevance to the general understanding of the structure-sensitivity pattern observed in several electrocatalytic bond-breaking and bond-making reactions.[1]

EXPERIMENTAL AND COMPUTATIONAL METHODS

Experimental Section. The working electrodes used for the experiments were platinum bead-type single-crystal electrodes of Pt[n(1 0 0) × (1 1 0)] orientation as well as Pt(1 1 1). The surfaces studied were Pt(1 0 0) with $n = \infty$, Pt(5 1 0) with $n = 5$ and Pt(10 1 0) with $n = 10$, which were prepared according to Clavilier's method.[20] The step density defined as $\theta_{step} = 1/n$ will be used in this study as a quantitative measure of the step concentration. Electrochemical measurements were carried out in a conventional three-electrode glass cell. All glassware was cleaned by boiling in a 1:1 mixture of concentrated nitric acid and sulfuric acid followed by repeated boiling with ultrapure water (Millipore Milli-Q A10 gradient, 18.2 MΩ cm, 2−4 ppb total organic content) before each experiment. In all experiments, a platinum wire was used as counter electrode. A reversible hydrogen electrode (RHE) was used as the reference electrode in all experiments. The supporting electrolyte, 0.1 M $HClO_4$, was prepared from concentrated perchloric acid (Merck, "Suprapur") and ultrapure water. Concentrations of ethanol (Merck, pro analyze) and DME were 0.5 and 1.65 M (which is the saturation concentration after bubbling DME for 15 min,[8] DME from Fluka, 99.9%), respectively. Argon (Air Products, "BIP Plus", 6.6) was used to deoxygenate all solutions. Prior to each experiment, the electrodes were flame annealed and cooled to room temperature (20 °C) in an argon−hydrogen mixture (ca. 3:1), after which they were transferred to the electrochemical cell under the protection of a droplet of deoxygenated ultrapure water.[21] Measurements were performed at room temperature using a computer-controlled Autolab PGSTAT 12 potentiostat (Ecochemie). The adsorbate-stripping experiments start by immersing the working electrode in the solution of 0.5 M ethanol or saturated DME in supporting electrolyte at a given potential (0.1∼0.6 V) for 5, 15, or 30 min, depending on the aim of the experiment to adsorb a certain amount of the dissociation products. Next, the electrode is transferred to a cell containing only supporting electrolyte and a cyclic voltammogram in the hydrogen underpotential deposition (H_{UPD}) region is recorded. The difference in the charge of the H_{UPD} region in the absence and presence of DME adsorbates allows us to calculate the amount of adsorbates. The adsorbates on the surface may be stripped off either reductively or oxidatively. For the stripping of reducible adsorbates, the electrode is held at 0 V for 5 min to remove the reducible fragments, followed by the recording of a voltammogram in the H_{UPD} region to determine the amount of sites freed by the reductive stripping, and subsequently an oxidative voltammetric sweep is recorded up to 0.85 V, to oxidize the adsorbates that were not stripped off the surface during the reductive stripping. For the purely oxidative stripping, the oxidative voltammetric sweep up to 0.85 V is performed directly after the recording of the H_{UPD} region. At the end of the experiment, a cyclic voltammogram between 0.1 and 0.45 V is recorded to ascertain that a clean adsorbate-free surface is obtained after the stripping processes. The coverages of the reducible and oxidizable fragments are calculated on the basis of the number of the blocked H_{UPD} sites. More detailed information on these procedures can be found in ref 17.

For Online Electrochemical Mass Spectrometry (OLEMS) and online HPLC measurements, the detailed experimental procedures can be found in refs 22 and 23. The OLEMS setup consists of a small inlet tip made of Peek into which a porous Teflon plug is pressed. The tip is connected to the mass spectrometer and is brought in close proximity (∼10 μm) to the electrode in the hanging meniscus configuration, by means of a micrometer positioning system and a camera. For HPLC measurements, the reaction products were collected with a small Teflon tip (0.38 mm inner diameter) positioned close (∼10 μm) to the center of the electrode surface, which was connected to a Peek capillary with inner/outer diameters of 0.13/1.59 mm. The tip is essentially identical to the tip that we developed for the OLEMS setup, with the only difference that no hydrophobic membrane is present inside the capillary in this case. Collected samples during voltammetry were analyzed offline by HPLC (Prominence HPLC, Shimadzu, equipped with an Aminex HPX 87-H (Biored) column for the detection of formaldehyde and formic acid).

Computational Section. The DFT calculations were performed with the VASP code.[24,25] We used PBE as exchange-correlation functional.[26] The wave functions were expanded in plane waves with a kinetic energy cutoff of 450 eV. The interaction between the ions and electrons was described by Projector Augmented Wave (PAW) potentials.[27,28] The periodically repeated simulation cells include slabs of five substrate layers, the topmost three of which and the adsorbates were relaxed whereas the atoms in the two bottom layers were fixed at their equilibrium bulk positions. The vacuum between the slabs is 13 Å. The unit cells used for Pt(1 0 0), Pt(2 1 0), Pt(3 1 0), Pt(4 1 0), and Pt(5 1 0) correspond to (3 × 3), (3 × 4), (3 × 3), (3 × 4), and (3 × 5) repetitions, respectively. Integration in the first Brillouin zone is performed using Monkhorst-Pack grids[29] including 5 × 5 × 1 k-points for Pt(1 0 0), Pt(2 1 0), Pt(4 1 0), and Pt(5 1 0) and 5 × 3 × 1 for Pt(3 1 0), respectively. In all calculations, the positions of the free atoms are optimized until the maximum force on any of them was less than 0.04 eV/Å. Convergence of energy differences with respect to the used cutoff energies and k-point grids was ensured within a tolerance of 10 meV/atom.

The binding energies of *CO on five Pt(n 1 0) surfaces were calculated (see Table S1 of the Supporting Information, SI). The *CO adsorption energy on the terrace was found to be not strongly dependent on the terrace width. As Pt(4 1 0) was found to have weak step−step interactions, it was chosen as the stepped surface for comparison to Pt(1 0 0). Since it is known that C_2 species dehydrogenate before internal C−C or C−O bonds are broken,[13,15,17,18] we restricted our DFT calculations of the DME adsorbates to $*CH_xOC$ ($x = 0, 1, 2, 3$) fragments, and to *CO and $*CH_x$, on Pt(1 0 0), Pt(4 1 0), and Pt(1 1 1). The influence of water solvation on the adsorption energies was not included, as it is expected to be similar for all species and will, thus, cancel out in the overall reaction. Figure 1 shows the Pt(1 0 0) and Pt(4 1 0) surfaces and the possible adsorption sites. The binding energies of species i (with i = $*CH_3OC$, $*CH_2OC$, *CHOC, and *COC) were computed as the reaction energies of the following process:

dx.doi.org/10.1021/ja406655q | J. Am. Chem. Soc. 2013, 135, 14329−14338

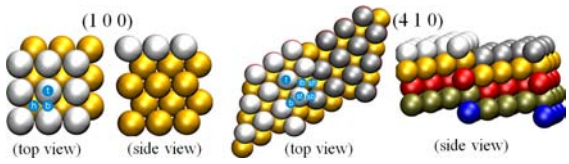

Figure 1. Schematics of Pt(1 0 0) and Pt(4 1 0). Marked are the possible adsorption sites: (h) hollow; (b) bridge; (t) top; (lb) long bridge; (sh) step hollow; (sb) step bridge; and (st) step top.

$$* + CH_3OCH_3 \rightarrow *CH_xOC + \frac{(6-x)}{2}H_2 \quad (1)$$

For convenience, we choose to represent the binding energies as follows:

$$\Delta E_{ads,i} = E_{surf,i} - E_{ref,i} \quad (2)$$

where $E_{surf,i} = E_{*i} - E_*$, is the surface-related part of the binding energies, and $E_{ref,i}$ is the reference energy of species i in gas-phase and is given by the following equation:

$$E_{ref,i} = E_{DME} - \frac{(6-x)}{2}E_{H_2} \quad (3)$$

The free energy of adsorption of species i is calculated from the following expression:

$$\Delta G_{ads,i} = \Delta E_{ads,i} + \Delta ZPE_i - T\Delta S_i \quad (4)$$

where ΔS_i and ΔZPE_i are the entropy and zero-point energy changes of reaction at T = 293 K. ΔZPE_i and ΔS_i are calculated using DFT calculations of the vibrational frequencies and standard thermodynamic tables for gas- phase molecules.[30,31] Vibrational contributions to the entropies of adsorbed species were also taken into account. The data needed for the computation of the free energies of adsorption of all intermediates on all surfaces can be found in the SI.

The transition states (TS) were determined with the Nudged Elastic Band (NEB) method.[32] Six images were generated between the initial state (IS) and the final state (FS) by a linear interpolation of the coordinates. Then the images were optimized simultaneously, and the saddle point was determined. The validity of the transition state found with the NEB method was verified through vibrational-frequency analyses by checking that the state had only a single imaginary frequency.

EXPERIMENTAL RESULTS

Cyclic Voltammetry. Most kinetic studies of the electrochemical oxidation of DME on Pt have been carried out in sulfuric acid.[13−15] Because of the strong interaction of SO_4^{2-} with Pt, perchloric acid ($HClO_4$) is a more suitable electrolyte for examining the surface structure sensitivity of the reaction kinetics.[33] Figure 2, parts (a) and (b), presents the cyclic voltammetry (CV) of the oxidation of DME and ethanol, respectively, on the different electrodes in 0.1 M $HClO_4$. To protect the electrodes, the positive potential limit is chosen as 0.9 V vs the reversible hydrogen electrode (RHE), to avoid the irreversible formation of surface oxides. Figure 2a shows the effect of introducing steps in Pt(1 0 0) terraces on the oxidation activity of DME. In the positive-going scan, a first peak appears in the range of 0.3−0.35 V (corresponding to hydrogen desorption[34]), followed by a sharp oxidation peak starting at 0.72 V. In the negative-going scan, there is only one peak centered at 0.67 V. The observation of the peak at 0.3−0.35 V in the positive-going scan indicates weak DME adsorption and that hydrogen is a competitive adsorbate during the adsorption process. In the negative-going scan, strongly adsorbed intermediates of DME oxidation block the hydrogen adsorption. Previous works on the oxidative adsorption of

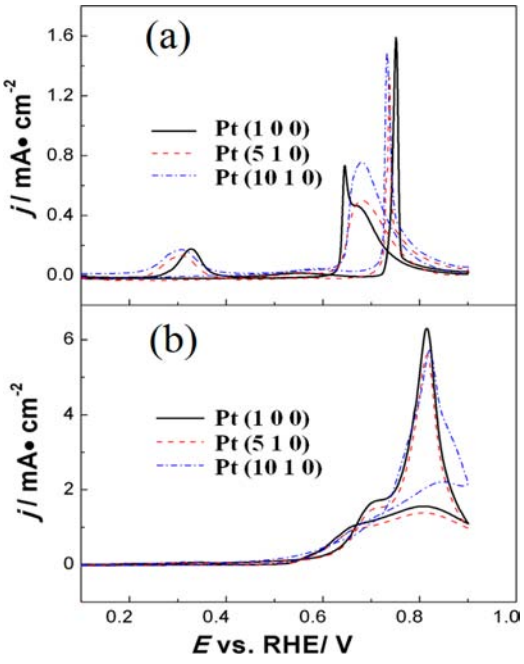

Figure 2. Cyclic voltammograms for the electro-oxidation of (a) saturated solution of DME in 0.1 M $HClO_4$, (b) 0.5 M ethanol in 0.1 M $HClO_4$ on Pt(1 0 0), Pt(5 1 0), and Pt(10 1 0). Scan rate: 50 mV s^{-1}.

DME have also suggested that DME adsorption is a slow process at low potential, initiated by C−H bond breaking as evidenced by the detection of $*CH_2OCH_3$ with in situ IR spectroscopy.[14,15] In general, the introduction of steps into Pt(1 0 0) surfaces tends to lower the activity, in agreement with the chronoamperometry experiments of Tong et al.,[8] though in those experiments, the effect is more significant than for the results shown in Figure 2(a).

Figure 2(b) shows the cyclic voltammetry of ethanol oxidation on the same electrodes. Current densities for ethanol are around 4 times higher than those for DME, even if the DME concentration is around three times higher, demonstrating that ethanol oxidation is a much faster reaction. For ethanol, the hydrogen region is completely suppressed due to the strong adsorption of its dissociation products. The oxidation peak starts with a shoulder appearing at 0.5 V and shows a maximum at 0.8 V. In the reverse scan, the oxidation current rises again, leading to a broad peak. Similar to DME, ethanol oxidation only shows small differences between different electrodes, but it is generally observed that steps decrease the oxidation performance.

Stripping Experiments. To confirm that the structure of the platinum surface impacts on the C−O bond-breaking step, we have performed stripping experiments to estimate the amount of bond-breaking fragments on the surface. Before presenting the detailed stripping results at different potentials and surfaces, we first describe an experiment that confirms the formation of reducible fragments during the dissociative adsorption of DME. In such an experiment, the electrode potential is kept at 0.4 V to generate adsorbed fragments. Next the electrode is held at 0 V for 5 min to remove any possible reducible fragments and subsequently scanned up to 0.85 V, or it is directly scanned up to 0.85 V without the prereduction period at 0 V. The difference between the two positive-going voltammetric sweeps is shown in Figure 3 and strongly suggests

dx.doi.org/10.1021/ja406655q | J. Am. Chem. Soc. 2013, 135, 14329−14338

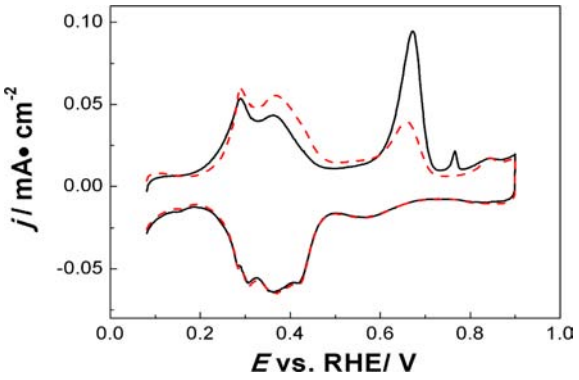

Figure 3. Voltammetry of the oxidative stripping of DME adsorbates in 0.1 M $HClO_4$ without (black —) and with (red -----) the reductive stripping by keeping the electrode at 0 V for 5 min. Scan rate: 50 mV s^{-1}.

the existence of reducible fragments. As shown in Figure 3, in case the reducible fragments have not been removed, there is a larger main oxidation peak at 0.67 V as well as a small oxidation peak at 0.76 V during the oxidative stripping of all adsorbates. The difference must be due to the presence of reducible fragments. As suggested by the ethanol stripping results reported previously,[17] the reducible fragments are *CH_x (most likely *CH, according to SERS experiments[18]) while the oxidizable fragment is *CO. The confirmation of the presence of *CH_x and the voltammetry of oxidative stripping of ethanol can be found in ref 18 and in Figure S2 of the SI.

Figure 4, parts (a) and (b), summarizes the stripping results of DME and ethanol, respectively, on Pt(1 0 0). The figure plots the hydrogen charge blocked by reducible fragments (i.e., *CH_x), oxidizable fragments (i.e., *CO), and their sum ("total" fragments), as a measure of their corresponding coverage due

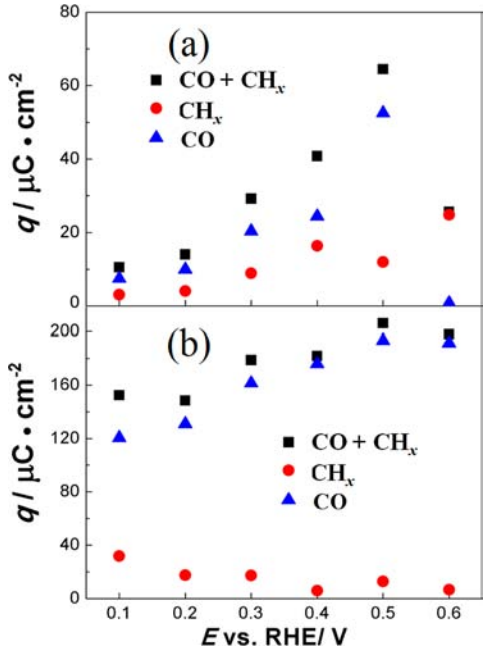

Figure 4. Oxidative stripping results for the following: (a) DME and (b) ethanol on Pt(1 0 0) in 0.1 M $HClO_4$ with the adsorption time of 15 min (for DME) and 5 min (for ethanol). Total amount of dissociated fragments (black ■); oxidizable fragments *CO (blue ▲); and reducible fragments *CH_x (red ●).

to the dissociative adsorption of either DME or ethanol. Examples of the voltammograms of the stripping process of DME and ethanol are shown in Figures S3 and S4 of the SI. As shown in Figure 4(a), small amounts of reducible and oxidizable fragments from DME can already be detected at potentials as low as 0.1 V, which indicates that dissociative adsorption of DME can take place even when hydrogen is adsorbed on the surface. There is an increase in the amount of total fragments up to 0.5 V. This potential dependent adsorption process suggests that the dissociative adsorption of DME on the electrode involves charge transfer. At 0.6 V, the amount of oxidizable species has dropped to nearly zero, which indicates that the oxidation of oxidizable species starts between 0.5 and 0.6 V. It is found that the onset potential for DME oxidation is 0.72 V (see Figure 2a). The observation that its dissociative *CO fragment can be oxidized above 0.5 V shows that the cleavage of the C−O bond is the rate-determining step for the direct DME oxidation. As to the reducible species, two interesting observations can be made from Figure 4a. The coverage corresponding to *CH_x increases with potential up to 0.4 V, but drops considerably at 0.5 V. It is proposed that around this potential, there is a transformation reaction from *CH_x to *CO during the dissociative adsorption. Second, at 0.6 V, only reducible adsorbates exist on the surface. Finally, we estimate that the highest coverage of adsorbed species is around $65/(n \times 209) \approx 0.16$ ML, where $n = 2$ (oxidation of CO to CO_2) and 209 μC cm^{-2} is the charge corresponding to a monolayer of adsorbed hydrogen. This low coverage of fragments confirms the slow dissociative adsorption of DME.

Figure 4(b) summarizes the stripping results of ethanol on Pt(1 0 0) with an adsorption time of 5 min at the various indicated potentials. It is found that the amount of oxidizable species increase with potential up to 0.5 V and show a slight decrease at 0.6 V, while the amount of reducible species decrease with potential over the entire potential range. Note that these trends agree with the literature reports of ethanol oxidation on other single-crystals.[17] Compared to DME, ethanol dissociation is considerably easier, leading to a much higher coverage of fragments. The decrease of the *CH_x coverage with increasing potential suggests that oxidation of *CH_x to *CO takes place at low potentials. However, *CO dissociated from ethanol is hardly oxidized at 0.6 V, while *CO from DME is more extensively oxidized at this potential. We believe that both observations may be due to coverage effects. It is well-known that a high coverage of CO on the surface (as in the case of ethanol) blocks sites for the adsorption of OH species, therefore requiring higher oxidation potentials.[35] Moreover, we speculate that a situation in which there are high coverages of *CH_x and *CO on the surface may favor the transformation of *CH_x into *CO, compared to a lower adsorbate coverage.

Figure 5 shows the results of DME stripping on Pt(1 1 1) provided for the sake of comparison with Pt(1 0 0). To make sure that the adsorption of DME fragments on Pt(1 1 1) was close to equilibrium, we extended the adsorption time to 30 min. As shown in Figure 5, no fragments are detected until 0.4 V, evidencing that the bond cleavage in DME is more difficult on Pt(1 1 1) than on Pt(1 0 0). Increasing the potential from 0.5 V to 0.7 V leads to a small amount of adsorbed fragments. In addition to the smaller total amount of fragments compared to Pt(1 0 0), Pt(1 1 1) exhibits the presence of more reducible species, suggesting a slower transformation of *CH_x into *CO.

dx.doi.org/10.1021/ja406655q | J. Am. Chem. Soc. 2013, 135, 14329−14338

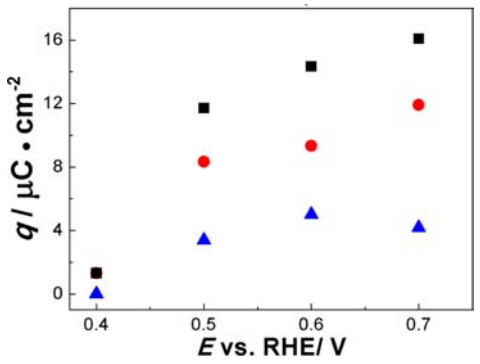

Figure 5. Stripping results for DME on Pt(1 1 1) in 0.1 M $HClO_4$ with an adsorption time of 30 min. Total amount of dissociated fragments (black ■); oxidizable fragments *CO (blue ▲); and reducible fragments *CH_x (red ●).

Figure 6, parts (a) and (b), compares the results of the stripping experiments of DME on Pt(1 0 0) with two stepped

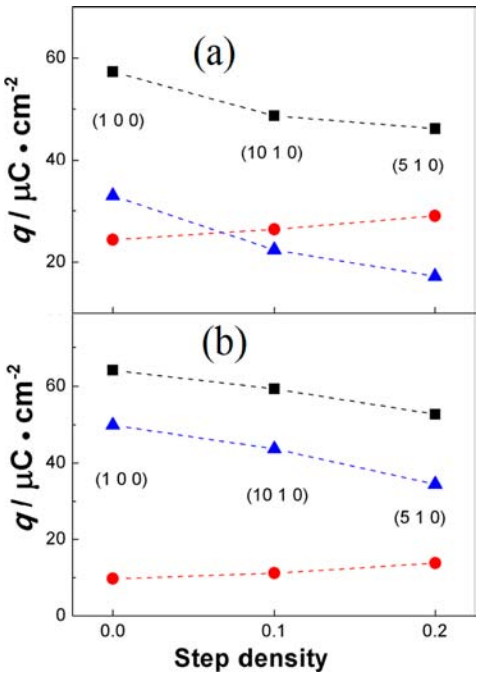

Figure 6. Oxidative stripping results for DME at an adsorption potential of 0.4 V in 0.1 M $HClO_4$ for different adsorption times: (a) 15 min, (b) 30 min, respectively. Total amount of dissociated fragments (black ■); oxidizable fragments *CO (blue ▲); and reducible fragments *CH_x (red ●).

surfaces, Pt(5 1 0) and Pt(10 1 0), for an adsorption potential of 0.4 V for two different adsorption times. Blank and stripping voltammograms of the stepped surfaces are given in Figures S5, S6, and S7 of the SI. As illustrated in Figure 6(a), the total amount of adsorbed species decreases with step density, showing that steps are not beneficial for the cleavage of the C−O bond. Interestingly, the amount of reducible fragments increases with step density. For an adsorption time of 15 min, it is found that on the stepped surfaces, the amount of reducible species is larger than the amount of oxidizable species. This suggests that the oxidation of *CH_x to *CO is either hindered at steps or occurs at a lower rate at steps, leading to a smaller amount of oxidizable fragments. Figure 6(b) shows that after prolonging the adsorption time to 30 min, there is a modest 10% increase in the total amount of adsorbed species for all three electrodes. Moreover, the amount of oxidizable fragments is now larger than the amount of reducible fragments, confirming that the oxidation reaction of *CH_x to *CO is slow. The conclusion drawn from Figure 6 is that steps are not active sites in the scission of the C−O bond and also that steps hinder the transformation of *CH_x to *CO.

Figure 7 plots the results of the stripping experiments on the different surfaces for the dissociative adsorption of ethanol at

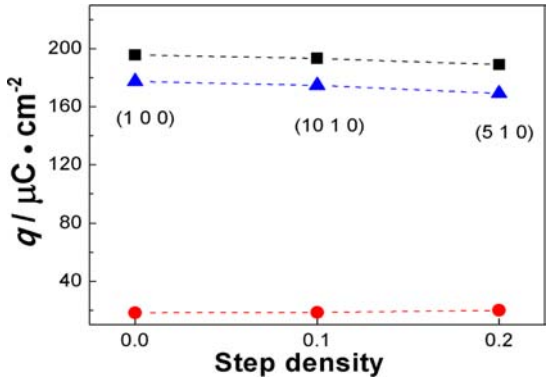

Figure 7. Oxidative stripping results for ethanol at an adsorption potential of 0.4 V in 0.1 M $HClO_4$ for 5 min. Total amount of dissociated fragments (black ■); oxidizable fragments *CO (blue ▲); and reducible fragments *CH_x (red ●).

0.4 V. Different from DME, introducing steps into Pt(1 0 0) has a much smaller influence on the bond scission. It can be seen that the amount of total fragments is almost the same for all three electrodes. Additionally, the amount of reducible fragments is always low, showing again that oxidation of *CH_x to *CO is much easier from ethanol than the oxidation of *CH_x generated by DME dissociation.

We note that for all our stripping experiments, the adsorption potential was limited to values below 0.6 V. Previous studies of DME electro-oxidation by FTIR[15] suggested that the dehydrogenation of DME takes place at low potentials (<0.6 V), and the cleavage of the C−O bond occurs at potentials higher than 0.6 V. One of the reasons why we detected the decomposition fragments at potentials below 0.6 V is that the coverages on Pt(1 0 0) are higher than on polycrystalline platinum as used for IR in ref 15. In addition, as Figure 6 shows, a prolonged adsorption time increases the detectable amount of fragments, proving that there is a time effect on the decomposition process. Therefore, in our experiments, the potential of 0.6 V corresponds to the onset of the oxidation of the adsorbed CO fragment, not to the onset of C−O bond breaking step.

To detect the volatile or dissolved intermediates and products during the DME oxidation process, both OLEMS and HPLC were employed. A large Pt(1 0 0) electrode (8 mm diameter) was used to improve detection. The only product observed was CO_2 at high oxidation potentials. We were unable to observe the formation of CH_4 from the reducible fragments *CH_x, which suggests that too few of such fragments exist to generate a detectable amount of CH_4. Significantly, HPLC did not detect formaldehyde or formic acid (potential oxidation products of methanol) as intermediates during DME oxidation. Therefore, we consider CO_2 to be the only nonadsorbed product of DME oxidation.

dx.doi.org/10.1021/ja406655q | J. Am. Chem. Soc. 2013, 135, 14329−14338

Table 1. Summary of the Free Energies of Adsorption of Adsorbates and Their Dissociation Fragments, Free Energies of the Bond-Breaking Step, and Free Energy of Activation of the Bond-Breaking Step on Pt(1 0 0) at U = 0 V[a]

adsorbate/fragments	ΔG_{ad} (eV)	$\Delta G_{reaction}$ (eV)[b]	$G_{barrier}$ (eV) [$E_{barrier}$/eV][b]	figure
CH_3OC/(CH_3 + *CO)	−0.19/−0.92	−0.73	1.19 [1.46]	8(a)
CH_2OC/(CH_2 + *CO)	0.20/−1.31	−1.51	0.20 [0.27]	8(b)
*CHOC/(*CH + *CO)	0.24/−1.63	−1.87	0.01 [0.05]	8(c)

[a]In the fourth column, the numbers in brackets correspond to the NEB barrier without any entropic or ZPE corrections. [b]$\Delta G_{reaction} = \Delta G_{ad,(CHx+CO)} - \Delta G_{ad,CHxOC}$ and $G_{barrier} = \Delta G_{ad,CHxOC\_TS} - \Delta G_{ad,CHxOC}$.

Figures 6 and 7 illustrate the different structure sensitivity of DME and ethanol oxidation. As we will confirm in the next section, the structure sensitivity of DME oxidation is rooted in the breaking of the C−O bond, which is the slow step. Conversely, the structure sensitivity of the oxidation of ethanol,[17] and also that of methanol,[36] is rooted in the dehydrogenation steps, i.e., the breaking of O−H and C−H bonds, to yield the corresponding aldehyde. Both ethanol and methanol oxidation on Pt are catalyzed by step and defect sites.

COMPUTATIONAL RESULTS

Reaction Process of *CH_xOC on Pt(1 0 0). On the basis of the present and previous experimental results on DME oxidation[15] and computational results on ethanol dehydrogenation,[37] we assume that the electrochemical oxidation of DME starts with the complete dehydrogenation of one of the methyl groups until the intermediate *CH_xOC (x = 0, 1, 2, or 3) is formed as the precursor of the C−O bond-breaking step. In the *CH_xOC adsorbate, either further dehydrogenation takes place, or the C−O bond is broken. The dehydrogenation reactions are thought to be electrochemical, i.e., a proton−electron pair is transferred between reactants and products:

$$*CH_xOC \rightarrow *CH_{x-n}OC + n(H^+ + e^-) \quad (5)$$

Since protons and electrons are transferred, the reaction energies depend on pH and the applied potential (U_{RHE}). Following the Computational Hydrogen Electrode model,[38] the free energies of the reaction steps are biased by $-neU$, where n is the total number of proton−electron pairs transferred, with n = 1 for a single step. The cleavage of the C−O bond is a purely chemical reaction, i.e., not electrochemical as proton−electron pairs are not involved and therefore, the electrode potential or the pH does not directly influence it.

Table 1 summarizes the free energies of adsorption of the various *CH_xOC fragments on Pt(1 0 0), the free energy of dissociation, and the kinetic barrier for the corresponding dissociation (bond-breaking) step, all at U = 0 V. The potential energy surfaces with images of the initial, transition, and final states are shown in Figure 8, parts (a)−(c). The phase diagram of the stable *CH_xOC fragments on Pt(1 0 0) as a function of potential is presented in Figure 9. Inspection of the binding energies of the *CH_xOC states shows that at U = 0 V, *CH_3OC is the most stable adsorbate on Pt(1 0 0). The *CH_2OC fragment becomes more stable than *CH_3OC at U = 0.20 − (−0.19) = 0.39 V, and *CHOC becomes more stable than the *CH_3OC fragment at (0.24 + 0.19)/2 = 0.22 V. We also considered the binding of *COC to Pt(1 0 0), which has the same adsorption geometry as *CHOC. *COC will be the most stable adsorbate on the surface only at U > 0.79 V (see Table S3 of the SI). On the basis of these DFT results, we conclude that in the experimental potential region of DME oxidation, *CHOC is the most stable adsorbate of the four possible *CH_xOC adsorbates. According to Figure 8 and Table 1, this species has also the lowest activation energy for dissociation and the highest thermodynamic driving force for

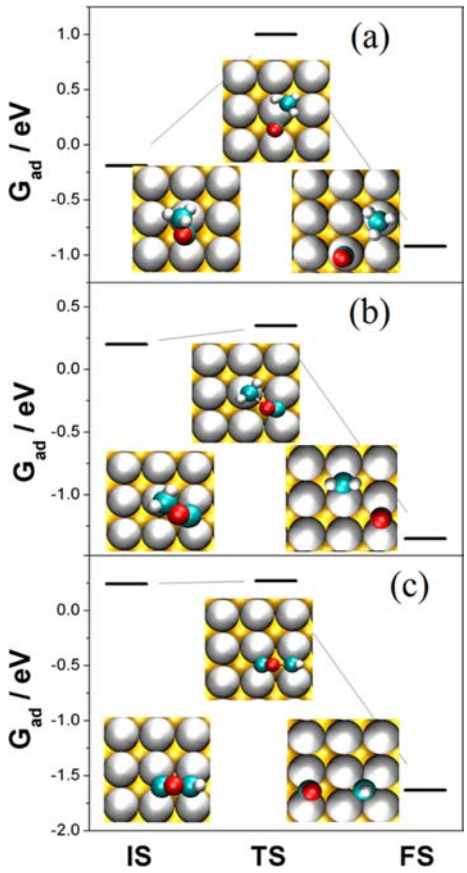

Figure 8. Free energies of the initial (IS), transition (TS) and final states (FS) for the bond-breaking steps of *CH_xOC on Pt(1 0 0) for the following: (a) *CH_3OC, (b) *CH_2OC, and (c) *CHOC. The insets show the corresponding relaxed geometries of each state. IS and FS are the most stable geometries.

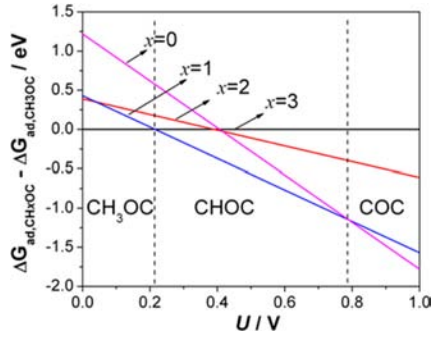

Figure 9. Stability of the different *CH_xOC species on Pt(1 0 0) as a function of the applied potential (U).

dx.doi.org/10.1021/ja406655q | J. Am. Chem. Soc. 2013, 135, 14329−14338

Table 2. Summary of the Free Energies of Adsorption of Adsorbates and Their Dissociation Fragments, Free Energies of the Bond-Breaking Steps, and Free Energy of Activation of the Bond-Breaking Steps on Pt(4 1 0) at U = 0 V[a]

adsorbate/fragments	ΔG_{ad} (eV)	$\Delta G_{reaction}$ (eV)[b]	$G_{barrier}$ (eV) [$E_{barrier}$/eV][b]	figure
CH_3OC/(CH_3 + *CO)	−0.12/−1.61	−1.73	1.21 [1.38]	10(a)
CH_2OC/(CH_2 + *CO)	0.25/−1.71	−1.96	0.05 [0.10]	10(b)
*CHOC/(*CH + CO)	0.32/−1.77	−2.09	0.02 [0.04]	10(c)

[a]In the fourth column, the numbers in brackets correspond to the NEB barrier without any entropic or ZPE corrections. [b]$\Delta G_{reaction} = \Delta G_{ad,(CHx+CO)} - \Delta G_{ad,CHxOC}$ and $G_{barrier} = \Delta G_{ad,CHxOC\_TS} - \Delta G_{ad,CHxOC}$.

breaking the C−O bond, as evidenced by the Brønsted−Evans−Polanyi (BEP) relation[39] in Figure S8 of the SI. The relation between barrier and reaction energy has a slope of 0.81, in excellent agreement with the universal relationship recently found by Wang et al. for dissociation reactions on transition metal surfaces.[40] Besides, the BEP line reveals an interesting feature of the Pt(1 0 0) surface: the barriers for cleaving C−O bonds decrease as the adsorbate is dehydrogenated. We will provide an explanation for this later through Bader analyses of the adsorbed states. It is also worth noting that the *CHOC adsorbs in a way such that it optimally benefits from the symmetry of the (1 0 0) terrace, as it binds to two parallel neighboring bridge sites, a geometry which does not exist on a (1 1 1) terrace due to its hexagonal symmetry.

Reaction Process of *CH_xOC on Pt(4 1 0). Table 2 lists the free energies of adsorption on Pt(4 1 0) step-edge sites of the various *CH_xOC fragments, and the free energies of dissociation with their corresponding reaction barriers, all at U = 0 V. It is important to distinguish between the step sites, that have the (1 1 0) orientation in the Pt(4 1 0) surface chosen here, and the step edge site, i.e., the (1 0 0)-type terrace site adjacent to the step site. The step site does not exhibit strong binding of *CH_xOC fragments (see Tables S6, S7 and S8 of the SI; ca. 1.8 eV weaker than *CHOC on (1 0 0) terrace), and will, therefore, not be considered. Additionally, the *COC species does not bind strongly at the step site. This section therefore only considers the binding of various intermediates to the step-edge site, with the images of the initial, transition, and final states shown in Figure 10, parts (a)−(c). Noticeably, the adsorption geometries for *CH_2OC and *CHOC are exactly the same as those on Pt(1 0 0) and involve only one step site. Regarding the adsorption energies, *CH_3OC is the most stable adsorbate among the *CH_xOC species on Pt(4 1 0) step-edge sites, at U = 0 V. The *CH_2OC fragment starts to be more stable than *CH_3OC at U = 0.25 − (−0.12) = 0.37 V, and *CHOC becomes more stable than *CH_3OC at (0.32 + 0.12)/2 = 0.22 V. Therefore, we expect that in the experimental potential region of interest for DME oxidation, *CHOC will be the most stable adsorbate of the three *CH_xOC species. This species has also the lowest activation energy and the highest thermodynamic driving force for breaking the C−O bond (see Table 2 and Figure 10). We found that although *CH_2OC and *CHOC have similar barriers (the difference is only 0.03 eV), *CHOC is more stable than *CH_2OC at the potentials of interest ($G_{ads,*CHOC} - G_{ads,\ *CH2OC}$ = 0.32 −0.25 − U, such that *CHOC is more stable for U > 0.07 V). Therefore, we conclude that at the experimental potential region in which the fragments are observed (U > 0.1−0.2 V), *CHOC is the most likely precursor for the bond-breaking step. Since *CHOC does not adsorb strongly at step sites, and the step edges do not provide significantly different adsorption energies compared to Pt(1 0 0) terraces, we conclude that the introduction of step sites is ineffective for the bond breaking process. This explains

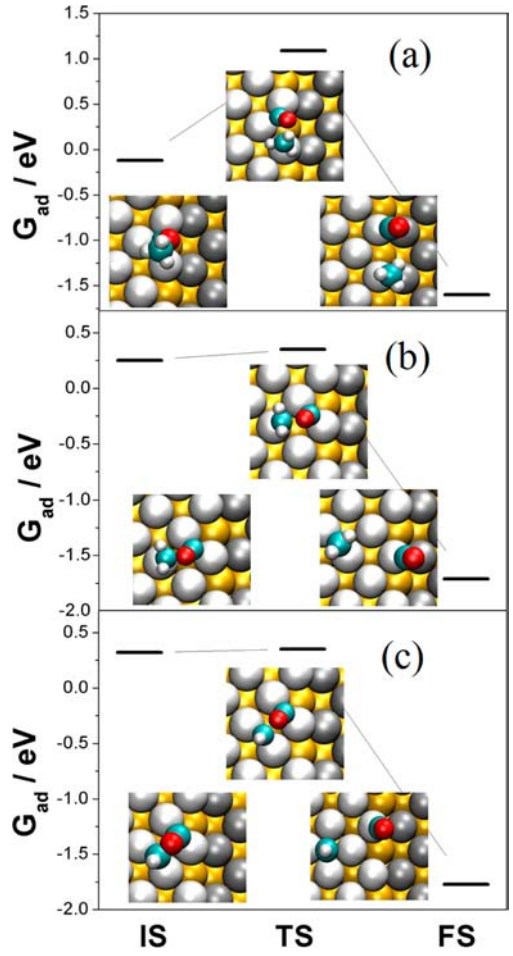

Figure 10. Free energies of the initial (IS), transition (TS), and final states (FS) for the bond-breaking steps of *CH_xOC on Pt(4 1 0) for the following: (a) *CH_3OC, (b) *CH_2OC, and (c) *CHOC. The insets show the corresponding converged geometries. IS and FS are the most stable geometries.

why the introduction of steps or defects in the (1 0 0) surface leads to a decrease in electrocatalytic activity. Note that this statement is primarily based on the idea that the key to the observed structure sensitivity lies in the favorable formation of the bond-breaking precursor, not in the bond breaking itself, but we also remark that the dissociation barriers for *CHOC are easily surmountable, which makes the cleavage of the C−O bond a straightforward process once the precursor is formed.

Noticeably, the coverage varies among the different facets. The experimental coverage is low (<0.16 ML) on Pt(1 0 0), lower for Pt(n 1 0) and much lower on Pt(1 1 1), as shown in Figures 5 and 6. These coverages do not correspond to a regime where significant adsorbate−adsorbate interactions are expected. Besides, the difference between the results on Pt(1 0

dx.doi.org/10.1021/ja406655q | J. Am. Chem. Soc. 2013, 135, 14329−14338

0) and Pt(4 1 0) is small, as shown in Tables 1 and 2. Additionally, the comparison is more focused on finding different features on the adsorption of *CH_xOC on Pt(1 0 0) or Pt(4 1 0), i.e., on square facets with and without defects. Therefore, we did not consider coverage effects in the calculations and we do not expect such effects to change the validity of the results.

DISCUSSION

Mechanism of the Electrochemical Oxidation of DME. The electrochemical oxidation of DME starts with the dissociative adsorption of DME. Compared to ethanol, DME oxidation is much slower, caused by the weak interaction of DME with the Pt substrate, leading to a low coverage on the surface and finally resulting in a much smaller oxidation current compared to that of ethanol. Moreover, the initial dehydrogenation of ethanol leads to a highly reactive intermediate, i.e., acetaldehyde.[17] The *CH_2OCH_3 surface intermediate is generated as the first adsorbed fragment of DME, as confirmed by IR.[14−16] Further dehydrogenation of *CH_2OCH_3 takes place to reach the critical fragment *CH_3OC. According to Ye et al., this fragment may hydrolyze to form CO and CH_3OH.[13] Since no formaldehyde and no formic acid were observed in our online HPLC experiments, which would be observable oxidation products of methanol, we believe that the formation of methanol is unlikely. Additionally, this observation excludes the cleavage of the C−O bond to form *CH_xO+*C. Besides, the experiments show no evidence for the formation of *C. Rather, our DFT results indicate that at the relevant oxidation potentials, the bond breaking precursor is *CHOC, which decomposes to the reducible fragment *CH and the oxidizable fragment *CO, both observed in the stripping experiments. No soluble byproduct has been found in the oxidation process, which strongly suggests that DME electro-oxidation generates only CO_2 and protons as final products. Consequently, the mechanism of electro-oxidation of DME is proposed as below:

$$CH_3OCH_3 \rightarrow *CH_3OC + 2(H^+ + e^-) \quad (6)$$

$$*CH_3OC \rightarrow *CHOC + 2(H^+ + e^-) \quad (7)$$

$$*CHOC \rightarrow *CH + *CO \quad (8)$$

$$*CH + H_2O \rightarrow *CO + 3(H^+ + e^-) \quad (9)$$

$$*CO + H_2O \rightarrow CO_2 + 2(H^+ + e^-) \quad (10)$$

In this mechanism, reaction step 8 is the structure-sensitive step, as it takes place preferentially on (1 0 0) terrace sites. In this mechanism, the intermediates that have been confirmed by IR are *CH_2OCH_3 and *CO.[15] Other intermediates, such as *$CHOCH_3$, *$COCH_3$, and *COCH, have not been detected, likely due to their short lifetime. *CH_x has been detected as a fragment of ethanol oxidation by SERS.[18] The similarity between the stripping characteristics of DME and ethanol fragments strongly indicates the presence of *CH_x during DME oxidation.

Why Pt(1 0 0) Is so Active. The DFT results presented above show that the ensemble of 4 neighboring atoms arranged in the square symmetry typical of (1 0 0) terraces, henceforth called "the active site", is the site where the bond scission takes place preferentially. That this site is indeed "the active site" is further supported by the electronic structure analysis of *CH_xOC on Pt(1 0 0) obtained by a Bader analysis. Figure 11 presents the number of valence electrons corresponding to the adsorbate atoms and the surface Pt atoms. The *CH_xOC fragments have intramolecular interactions, i.e., C−H and C−O bonds and "extramolecular" interactions, i.e., C-surface bonds. Breaking the C−O bond can be regarded as a competition between intramolecular and extramolecular interactions. Noticeably, as *CH_3OC is dehydrogenated to *CH_2OC and *CHOC, the number of intramolecular bonds decreases while the extramolecular bonds increase accordingly, in order to maintain the bond order of the adsorbates. According to the scaling relationships between species with different degrees of hydrogenation,[41] the binding energies are stronger for highly dehydrogenated species. An effective-medium-theory approach also predicts that the interaction with the surface should be stronger for the adsorbates that are more dehydrogenated due to the lack of bonds, which also explains the choice of different adsorption sites.[42] As shown in Figure 11, since C and O have 4 and 6 valence electrons, the *CO moiety is negatively charged in all cases (0.75 e^-, 0.63 e^-, and 0.80 e^- in *CH_3OC, *CH_2OC, and *CHOC, respectively). However, there is also a lack of electronic charge on the *CH_x moieties of 0.69 e^-, 0.42 e^-, and 0.41 e^- in *CH_3OC, *CH_2OC, and *CHOC, respectively. Therefore, the excess charge on the *CO moiety comes from the surface, i.e., 0.07 e^- for *CH_3OC, 0.21 e^- for *CH_2OC, and 0.39 e^- for *CHOC. Thus, for *CH_3OC, the 0.75 e^- in *CO are divided in 0.69 e^- from *CH_3 and 0.07 e^- from the surface. For *CH_2OC, the extra 0.63 e^- in *CO are divided in 0.42 e^- from *CH_2 and 0.21 e^- from the surface. Finally, the extra 0.80 e^- in the *CO moiety in *CHOC are divided in 0.41 e^- from *CH and 0.39 e^- from the surface. From this comparison, it is clear that the interaction between *CO and *CH_3 moieties is strong, moderate between *CO and *CH_2, and weak between *CO and *CH. The interaction between the *CO moieties and the surface goes in the opposite direction. It is also important to note that for *CH_3OC, *CH_2OC, and *CHOC the surface charge is donated by two, three and four Pt atoms, respectively, due to the different adsorption configurations. On average, the surface is donating 0.07, 0.07, and 0.10 e- per Pt atom, meaning that the surface atoms are providing approximately the same amount of charge in all cases and that the difference from one case to the next is due to the participation of more surface atoms. Moreover, the

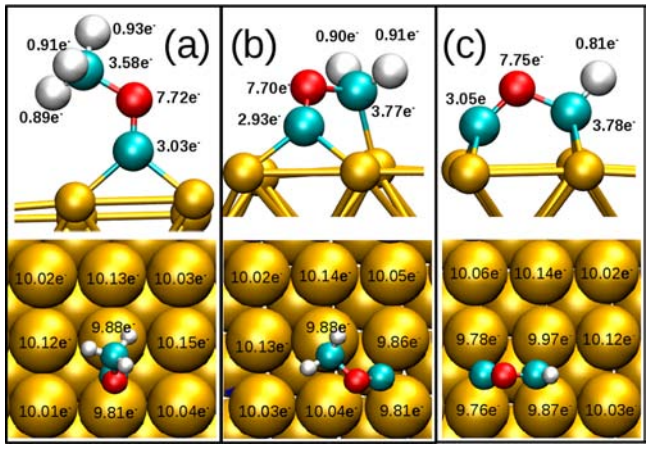

Figure 11. Counting of valence electrons per atom for *CH_xOC adsorbed on Pt(1 0 0), obtained through Bader analyses. (a) *CH_3OC; (b) *CH_2OC; and (c) *CHOC.

dx.doi.org/10.1021/ja406655q | J. Am. Chem. Soc. 2013, 135, 14329−14338

"active site" made of two opposing bridge sites provides the optimal geometry for anchoring the *CH and *CO moieties in the *CHOC initial and transition states with a minimum of internal repulsion as the *CH and *CO adsorbates are not bound to the same surface atoms.[43] Thus, the "active sites" provide both geometric and electronic symmetry that allows for more surface donation of charge at a low expense for each surface atom. The conjunction of both results is a compromise between the strengths of CO−CH and CO-surface interactions that facilitates the breaking of the C−O bond (0.41 vs 0.39 e^-). This is not the case for *CH_2OC or *CH_3OC. In the former the charged dragged from *CH_2 to *CO is twice that drained from the surface (0.42 vs 0.21 e^-). In the latter, the charge drained from *CH_3 is ten times as large as the one drained from the surface (0.69 vs 0.07 e^-).

For Pt(1 1 1) we found that *CH_3OC, *CH_2OC, and *CHOC binds to two, three, and three surface Pt atoms, and the free energies of adsorption are 0.3 eV, 0.63, and 1.55 eV, respectively, much weaker than those on Pt(1 0 0) (see Tables S5 and S10 of the SI). Thus, the appearance of *CH_2OC and *CHOC requires overpotentials of 0.79 and 0.83 V, respectively, which are around 0.5 V higher than that on Pt(1 0 0) (see Table S3 of the SI). This is in agreement with the experimental stripping results, which showed that the onset potential for generating the bond breaking fragments of DME on Pt(1 1 1) is around 0.4 V higher than that on Pt(1 0 0). As a result, Pt(1 1 1) shows a much lower electrocatalytic activity than Pt(1 0 0).

Assuming that the electrochemical oxidation of DME takes place mostly at (1 0 0) terraces, i.e., that the "active site" is the only place where the reaction takes place, it is possible to count the number of such sites on a given surface and relate them to the electrocatalytic activity. For a perfect (1 0 0) surface, the number of (1 0 0) terrace sites is given by the following equation:

$$N_{as,100} = 1/d^2 \tag{11}$$

where d is the average distance between two Pt atoms (0.278 nm). For surfaces with (1 1 0) or (1 1 1) step sites, with a terrace atom width n, the two rows of terrace sites near the steps (upper and lower step sites) do not contribute effective active sites. If the step sites themselves are considered inactive, then the number of active sites is approximately given by the following:

$$N_{as,n} \approx [(n-2)/n]^* N_{as,100} = (1-2/n)^* N_{as,100} = (1-2\theta_{step})/d^2 \tag{12}$$

Although this is clearly a rough model, it captures the strong dependence of $N_{as,n}$ on the step density θ_{step} or, conversely, the terrace width n. For instance, for a terrace width of 4 atoms, namely a (410) surface, the activity is expected to be half that of a (1 0 0) surface. For other reactions with a similar surface structural preference for the (1 0 0) terrace, we expect a similar model to be applicable.

We are not aware of any similar widespread structure sensitivity trend for heterogeneously catalyzed reactions. However, there are some indications in the literature about the special reactivity of (1 0 0) sites. For the gas-phase ammonia oxidation on platinum single crystals, Weststrate et al.[44] have pointed out the special reactivity of (1 0 0) terrace sites. Even closer to the present work, Qe and Neurock[45] carried out DFT calculations of NO dissociation on Pt(1 0 0), Pt(2 1 1), and Pt(4 1 0), and concluded that the square arrangement of the atoms produced the most active site for N−O bond breaking.

CONCLUSIONS

We have studied the structural dependence of the dissociation of DME on Pt single-crystal electrodes by electrochemical and computational methods. Our experiments confirmed that Pt(1 0 0) electrodes possess the largest electrocatalytic activity for DME oxidation. Furthermore, stripping experiments showed that step sites in (1 0 0) terraces are not active for breaking the C−O bond in DME and that steps hinder the transformation of *CH_x to *CO. The DFT results showed that this unique structure sensitivity stems from the fact that the preferred precursor species before breaking the C−O bond is a *CHOC adsorbate that prefers to bind to two opposing bridge sites, a symmetry only existing on (1 0 0) terraces. Steps or defects induce a discontinuity in the "active" structure of the two-dimensional (1 0 0) terrace, leading to a concomitant decrease in the total activity. On the basis of these results, the mechanism of the electrochemical oxidation of DME on Pt(1 0 0) is proposed to start with dehydrogenation steps until the *CHOC adsorbate is produced. The C−O bond of this intermediate is cleaved to form *CO and *CH fragments, which are finally oxidized to CO_2. More importantly, the identification of the active site consisting of a square arrangement of 4 surface atoms on the (1 0 0) terrace as the site that makes or breaks bonds, or equivalently, as the site that optimally stabilizes the intermediate(s) that act as the precursor state to the bond making and breaking, naturally explains the unique activity of the (1 0 0) surface for bond making and breaking reactions in electrocatalysis.[1] This important insight gives the fundamental atomic-scale underpinning of the enhancement of the electrocatalytic activity through surface structure engineering.

ASSOCIATED CONTENT

Supporting Information

Further results of stripping experiments and adsorption geometries and energies of *CH_xOC, *CH_x, and *CO; co- and separate adsorption of *CH_x and *CO on Pt(1 0 0) and Pt(4 1 0); adsorption geometries/energies of *CH_xOC on Pt(1 1 1); and entropies and ZPE of various fragments and gas phase molecules. This material is available free of charge via the Internet at http://pubs.acs.org.

AUTHOR INFORMATION

Corresponding Author

m.koper@chem.leidenuniv.nl

Notes

The authors declare no competing financial interest.

ACKNOWLEDGMENTS

This work was supported by the Chinese Scholarship Council (CSC) through a CSC Scholarship awarded to H.L., The Netherlands Organization for Scientific Research (NWO), the National Research School Combination Catalysis (NRSC-C, The Netherlands), and the Smart Mix Program of The Netherlands Ministry of Economic Affairs and The Netherlands Ministry of Education, Culture and Science, (research performed within the Catchbio program). The Stichting

Nationale Computerfaciliteiten (National Computing Facilities Foundation, NCF) is gratefully acknowledged for the use of their supercomputer facilities, with financial support from NWO. Y.L. thanks the National 2011 Program of China via the Tianjin Co-innovative Research Center of Chemical Science and Engineering and the Natural Science Foundation of China under Contract No. 21120102039.

REFERENCES

(1) Koper, M. T. M. *Nanoscale* **2011**, *3*, 2054.
(2) Calle-Vallejo, F.; Koper, M. T. M. *Angew. Chem., Int. Ed.* **2013**, *52*, 7282.
(3) Schouten, K. J. P.; Qin, Z. S.; Gallent, E. P.; Koper, M. T. M. *J. Am. Chem. Soc.* **2012**, *134*, 9864.
(4) Schouten, K. J. P.; Gallent, E. P.; Koper, M. T. M. *ACS Catal.* **2013**, *3*, 1292.
(5) Vidal-Iglesias, F. J.; Solla-Gullón, J.; Montiel, V.; Feliu, J. M.; Aldaz, A. *J. Phys. Chem. B.* **2005**, *109*, 12914.
(6) Ye, S.; Hattori, H.; Kita, H. *Ber.Bunsen-Ges. Phys. Chem.* **1992**, *96*, 1884.
(7) Duca, M.; Figueiredo, M. C.; Climent, V.; Rodríguez, P.; Feliu, J. M.; Koper, M. T. M. *J. Am. Chem. Soc.* **2011**, *133*, 10928.
(8) Tong, Y.; Lu, L.; Zhang, Y.; Gao, Y.; Yin, G.; Osawa, M.; Ye, S. *J. Phys. Chem. C.* **2007**, *111*, 18836.
(9) Strbac, S.; Anastasijevic, N. A.; Adzic, R. R. *J. Electroanal. Chem.* **1992**, *323*, 179.
(10) Lu, L.; Yin, G.; Tong, Y.; Zhang, Y.; Gao, Y.; Osawa, M.; Ye, S. *J. Electroanal. Chem.* **2008**, *619−620*, 143.
(11) Muller, J. T.; Urban, P. M.; Holderich, W. F.; Colbow, K. M.; Wilkinson, D. P. *J. Electrochem. Soc.* **2000**, *147*, 4058.
(12) Mench, M. M.; Chance, H. M.; Wang, C. Y. *J. Electrochem. Soc.* **2004**, *151*, A144.
(13) Lu, L.; Yin, G.; Tong, Y.; Zhang, Y.; Gao, Y.; Osawa, M.; Ye, S. *J. Electroanal. Chem.* **2010**, *642*, 82.
(14) Liu, Y.; Muraoka, M.; Mitsushima, S.; Ota, K.; Kamiya, N. *Electrochim. Acta* **2007**, *52*, 5781.
(15) Zhang, Y.; Lu, L.; Tong, Y.; Osawa, M.; Ye, S. *Electrochim. Acta* **2008**, *53*, 6093.
(16) Shao, M. H.; Warren, J.; Marinkovic, N. S.; Faguy, P. W.; Adzic, R. R. *Electrochem. Commun.* **2005**, *7*, 459.
(17) Lai, S. C. S.; Koper, M. T. M. *Faraday Discuss.* **2008**, *140*, 399.
(18) Lai, S. C. S.; Kleijn, S. E. F.; Rosca, V.; Koper, M. T. M. *J. Phys. Chem. C.* **2008**, *112*, 19080.
(19) Lai, S. C. S.; Koper, M. T. M. *J. Phys. Chem. Lett.* **2010**, *1*, 1122.
(20) Clavilier, J.; Armand, D.; Sun, S. G.; Petit, M. *J. Electroanal. Chem.* **1986**, *205*, 267.
(21) Lebedeva, N. P.; Koper, M. T. M.; Feliu, J. M.; Santen, R. A *Electrochem. Commun.* **2000**, *2*, 487.
(22) Wonders, A. H.; Housmans, T. H. M.; Rosca, V.; Koper, M. T. M. *J. Appl. Electrochem.* **2006**, *36*, 1215.
(23) Kwon, Y.; Koper, M. T. M. *Anal. Chem.* **2010**, *82*, 5420.
(24) Kresse, G.; Hafner, J. *Phys. Rev. B* **1993**, *47*, 1.
(25) Kresse, G.; Furthmuller, J. *Phys. Rev. B* **1996**, *54*, 11169.
(26) Perdew, J. P.; Burke, K.; Ernzerhof, M. *Phys. Rev. Lett.* **1996**, *77*, 3865.
(27) Blochl, P. E. *Phys. Rev. B* **1994**, *50*, 17953.
(28) Kresse, G.; Joubert, D. *Phys. Rev. B* **1999**, *59*, 1758.
(29) Monkhorst, H.; Pack, J. D. *Phys. Rev. B* **1976**, *13*, 5188.
(30) Rossmeisl, J.; Qu, Z.-W.; Zhu, H.; Kroes, G.-J.; Nørskov, J. K. *J. Electroanal. Chem.* **2007**, *1−2*, 83.
(31) Lide, D. R., Ed. *CRC Handbook of Chemistry and Physics*, 90th ed.; CRC Press: Boca Raton, FL., 2010, Section 5, pp 801−710.
(32) Jónsson, H.; Mills, G.; Jacobsen, K. W. In *Classical and Quantum Dynamics in Condensed Phase Simulations*; Berne, B. J., Ciccotti, G., Coker, D. F., Eds.; World Scientific: Hackensack, NJ, 1998; pp 385−404.
(33) Snell, K. D.; Keenan, A. G. *Electrochim. Acta* **1982**, *27*, 1683.
(34) Garcia-Araez, N.; Lukkien, J. J.; Koper, M. T. M.; Feliu, J. M. *J. Electroanal. Chem.* **2006**, *588*, 1.
(35) Lebedeva, N. P.; Koper, M. T. M.; Herrero, E.; Feliu, J. M.; van Santen, R. A. *J. Electroanal. Chem.* **2000**, *487*, 37.
(36) Housmans, T. H. M.; Koper, M. T. M. *J. Phys. Chem. B* **2003**, *107*, 8557.
(37) Ferrin, P.; Simonetti, D.; Kandot, S.; Kunkes, E.; Dumesic, J. A.; Nørskov, J. K.; Mavrikakis, M. *J. Am. Chem. Soc.* **2009**, *131*, 5809.
(38) Nørskov, J. K.; Rossmeisl, J.; Logadottir, A.; Lindqvist, L.; Kitchin, J. R.; Bligaard, T.; Jónsson, H. *J. Phys. Chem. B.* **2004**, *108*, 17886.
(39) Bligaard, T.; Nørskov, J. K.; Dahl, S.; Matthiesen, J.; Christensen, C. H.; Sehested, J. *J. Catal.* **2004**, *224*, 206.
(40) Wang, S.; Temel, B.; Shen, J.; Jones, G.; Grabow, L.; Studt, F.; Bligaard, T.; Abidl-Pedersen, F.; Christensen, C. H.; Nørskov, J. K. *Catal. Lett.* **2011**, *141*, 370.
(41) Abild-Pedersen, F.; Greeley, J.; Studt, F.; Munter, T. R.; Moses, P. G.; Skúlason, E.; Bligaard, T.; Nørskov, J. K. *Phys. Rev. Lett.* **2007**, *99*, 016105−016111.
(42) Jacobsen, K. W.; Nørskov, J. K.; Puska, M. J. *Phys. Rev. Lett.* **1987**, *35*, 7423.
(43) Van Santen, R. A. *Acc .Chem. Res.* **2009**, *42*, 57.
(44) Weststrate, C. J.; Bakker, J. W.; Rienks, E. D. L.; Vinod, C. P.; Matveev, A. V.; Gorodetskii, V. V.; Nieuwenhuys, B. E. *J. Catal.* **2006**, *242*, 184.
(45) Ge, Q.; Neurock, M. *J. Am. Chem. Soc.* **2004**, *126*, 1551.